In Situ Fixation Redefines Quiescence and Early Activation of Skeletal Muscle Stem Cells

Léo Machado, Joana Esteves de Lima, Odile Fabre, Caroline C. Proux, Rachel Legendre, Anikó Szegedi, Hugo Varet, Lars Roed Ingerslev, Romain Barrès, Frédéric Relaix, et al.

Cell Reports

Resource

In Situ Fixation Redefines Quiescence and Early Activation of Skeletal Muscle Stem Cells

Graphical Abstract

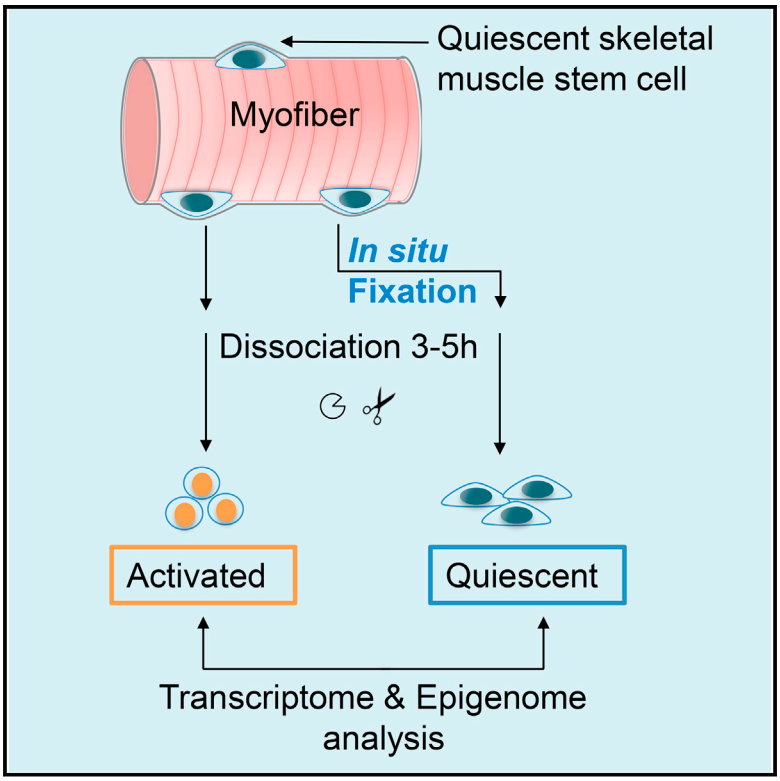

Authors

Léo Machado, Joana Esteves de Lima, Odile Fabre, ..., Romain Barrès, Frédéric Relaix, Philippos Mourikis

Correspondence

frederic.relaix@inserm.fr

In Brief

Machado et al. demonstrate that muscle stem cells undergo changes in transcripts and histone modifications during isolation. The authors develop an *in situ* fixation-based methodology, which allows capture of cells in their native state. In light of these findings, some high-throughput analyses of tissue extracted cells may need to be revisited.

Highlights

- Quiescent muscle stem cells undergo major transcriptomic alterations during isolation
- Isolation induces histone H3 modifications but leaves intact DNA methylation
- *In situ* fixation allows isolation of quiescent cells in their native, *in vivo* state
- *In situ* fixation detects quiescence and early activation factors

Data and Software Availability

GSE103162
GSE103163
GSE104543
GSE103164

Machado et al., 2017, Cell Reports *21*, 1982–1993
November 14, 2017
https://doi.org/10.1016/j.celrep.2017.10.080

CellPress

OPEN ACCESS
CellPress

Cell Reports
Resource

In Situ Fixation Redefines Quiescence and Early Activation of Skeletal Muscle Stem Cells

Léo Machado,[1] Joana Esteves de Lima,[1,5] Odile Fabre,[2,5] Caroline Proux,[3] Rachel Legendre,[3,4] Anikó Szegedi,[1] Hugo Varet,[3,4] Lars Roed Ingerslev,[2] Romain Barrès,[2] Frédéric Relaix,[1,6,*] and Philippos Mourikis[1]

[1]Biology of the Neuromuscular System, INSERM IMRB U955-E10, UPEC, ENVA, EFS, Creteil 94000, France
[2]Novo Nordisk Foundation Center for Basic Metabolic Research, Faculty of Health and Medical Sciences, University of Copenhagen, Copenhagen, Denmark
[3]Institut Pasteur, Plate-forme Transcriptome & Epigenome, Biomics, Centre d'Innovation et Recherche Technologique (Citech), Paris, France
[4]Institut Pasteur, Hub Bioinformatique et Biostatistique, Centre de Bioinformatique, Biostatistique et Biologie Intégrative (C3BI, USR 3756 IP CNRS), Paris, France
[5]These authors contributed equally
[6]Lead Contact
*Correspondence: frederic.relaix@inserm.fr
https://doi.org/10.1016/j.celrep.2017.10.080

SUMMARY

State of the art techniques have been developed to isolate and analyze cells from various tissues, aiming to capture their *in vivo* state. However, the majority of cell isolation protocols involve lengthy mechanical and enzymatic dissociation steps followed by flow cytometry, exposing cells to stress and disrupting their physiological niche. Focusing on adult skeletal muscle stem cells, we have developed a protocol that circumvents the impact of isolation procedures and captures cells in their native quiescent state. We show that current isolation protocols induce major transcriptional changes accompanied by specific histone modifications while having negligible effects on DNA methylation. In addition to proposing a protocol to avoid isolation-induced artifacts, our study reveals previously undetected quiescence and early activation genes of potential biological interest.

INTRODUCTION

The microenvironment of a cell can have a major impact on its properties. Both during physiological and pathological conditions, cell-to-cell contacts, paracrine signaling, oxygen and nutrient availability, extracellular matrix, and mechanical stress impact cells and influence their behavior (Rojas-Ríos and González-Reyes, 2014). This is especially true for stem cells, which, due to their plasticity, can radically alter their proliferation and differentiation state in response to changes in their niche. Based on this premise, a large number of studies have used cells directly isolated from the tissue of interest instead of using cultured or otherwise manipulated cells. However, the extent and nature of the actual modifications that arise in cells during the isolation procedure are unknown, calling into question whether analyses reported to date fully reflect the physiological status.

Adult stem cells can assume different cellular states, either quiescent or proliferating (Liu and Clevers, 2010). Quiescent stem cells are arrested in a reversible, non-cycling phase, and the cellular and molecular mechanisms that maintain this state remain largely undetermined. To understand these mechanisms, it is important to obtain a precise view of the transcriptomic and epigenetic landscapes of these cells present in their native *in vivo* state. With this goal, we have developed a protocol that relies on paraformaldehyde (PFA) fixation of the tissue prior to cell isolation, enabling capture of the molecular state of the cells as found in their niche. We have applied this *in situ* fixation technique to skeletal muscle stem cells (MuSCs), which are an indispensable stem cell population for regenerating injured or diseased muscle as well as maintaining tissue homeostasis (Zammit et al., 2004). Adult MuSCs are G0 arrested, and their quiescent niche is largely defined by a confined anatomical location, as these cells are positioned between the membrane of the myofiber and the overlying basement membrane. Disturbance of the niche, which occurs during muscle injury or experimental extraction, triggers activation of the MuSCs. Activation is manifested by an exit from G0 into a prolonged G1-phase (25–35 hr) (Mourikis et al., 2012; Rocheteau et al., 2012), phosphorylation of p38α/β mitogen-activated protein kinase, expression of the muscle regulatory factor MYOD (Jones et al., 2005; Zhang et al., 2010), and an increase in cellular volume (Rodgers et al., 2014). Therefore, MuSCs provide a suitable model for investigating the putative consequences of isolation procedures on the molecular signature of a cell.

In this study, we show that massive changes in transcript composition occur during MuSC purification. These changes do not involve alterations in DNA methylation but are associated with histone H3 modifications. By eliminating isolation-induced artifacts, we provide a precise quiescence signature of MuSCs and also identify putative regulators of early activation. Finally, this study describes an efficient and affordable method to isolate molecularly preserved cells amenable to

whole-genome analyses that could be applicable to a broad range of cell types.

RESULTS

Analysis of G0-Fixed MuSCs Isolated with the *In Situ* Fixation Protocol

For the isolation of MuSCs using standard protocols, muscles are dissected, mechanically minced into 1- to 2-mm pieces, and subsequently incubated with proteolytic enzymes at 37°C for up to 2 hr to allow detachment of the myofiber bundles and dissociation of the MuSCs (Figure 1A). Following several steps of washes and filtrations, MuSCs are isolated by fluorescence-activated cell sorting (FACS), based on specific plasma membrane receptors or genetically expressed fluorescent markers (Liu et al., 2015).

In order to isolate quiescent MuSCs, muscles were fixed *in situ* by ice-cold 0.5% PFA before cell dissociation (Figure 1A; Supplemental *In Situ* Fixation Protocol; Supplemental Experimental Procedures). We refer to these fixed cells as time-zero stem cells (T0-SCs) and the cells isolated by the standard 3-hr-long protocol as T3-SCs. We applied both the standard and the *in situ* fixation protocols for the isolation of MuSCs from transgenic *Tg:Pax7-nGFP* mice, in which nuclear GFP is expressed in MuSCs (Sambasivan et al., 2009) (Figure 1B). The purity of the isolated fixed cells was assessed by PAX7 staining and was similar to that of the cells isolated using the standard protocol (94% ± 3.1% and 92% ± 1.4% of $PAX7^+$ cells for T3- and T0-SCs, respectively; Figure S1A). Notably, equivalent numbers of GFP^+ cells were isolated from fixed and fresh muscles, indicating that *in situ* fixation did not lead to loss of cells (Figures 1B and S1B).

To ensure that the T0-SCs had been properly fixed and were biologically inert, we assessed their proliferation capacity by measuring incorporation of 5-ethynyl-2′-deoxyuridine (EdU), *de novo* RNA synthesis by the presence of the modified nucleotide ethynyl uridine (EU), and uptake of DAPI, a compound actively excluded from live cells. As expected for fixed cells, the T0-SCs did not incorporate EdU (Figure 1C), were transcriptionally inactive (Figure 1D), and were positive for DAPI (Figures S1C and S1D). Of note, the light scattering of T0-SCs was drastically different compared to the non-fixed T3-SCs, suggesting differences in the morphological complexity of the isolated cells. Indeed, MuSCs have a small cytoplasmic/nuclear ratio and *in vivo* are spindle shaped, with multiple branches emanating from their poles. Upon detachment from the myofibers, the stretched plasma membrane retracts to form small, round, uniform cells (Figure 1B, bottom left). Instead, when fixed, the dissociated MuSCs exhibit a complex morphology (Figure 1B, bottom right), possibly reflecting that found *in vivo*, as has been shown for fixed cardiomyocytes (Mollova et al., 2013). To confirm the differences in cell shape inferred from light scattering, we used the lectin marker WGA (wheat germ agglutinin) to stain cell membranes of T0- and T3-SCs (Figure 1E). Using an image-processing software (see Experimental Procedures), we calculated the mean eccentricity of T0- and T3-SCs, a circle having an eccentricity of 0 and a straight line of 1. Interestingly, we found that *in situ* fixed T0-SCs have a mean eccentricity significantly greater than that of T3-SCs (0.80 ± 0.009 versus 0.40 ± 0.013), corroborating that *in situ* fixation retains the physiological spindle shape of MuSCs that is lost during the conventional dissociation protocol (Figure 1E).

In summary, we have developed a protocol that allows efficient isolation of MuSCs from fixed tissue, with comparable purity and yield to those of non-fixed muscles. Moreover, we show that the cells isolated from PFA-treated samples are efficiently fixed and, hence, safeguarded from the strong stimuli to which they are exposed during the dissociation procedure.

PFA Fixation Does Not Alter mRNA Yield, Quality, and Composition

Having developed a method to isolate a highly pure population of *in situ* fixed MuSCs, we then sought to analyze its transcriptional profile. First, however, a series of experiments was performed to measure the putative effects of PFA fixation on mRNA quality and composition. As shown in Figure 2A, fresh muscles from *Tg:Pax7-nGFP* mice were digested, and GFP^+ MuSCs were isolated by FACS. Subsequently, half of the sorted MuSCs were immediately lysed, and the other half were fixed in 0.5% PFA before being lysed for RNA extraction. Of note, RNA extraction from fixed cells was optimized (Experimental Procedures), as standard protocols were not suitable (data not shown). We found that the RNA quality was not compromised by fixation, as the RNA integrity numbers (RINs) were similar between the fixed and non-fixed T3-SCs (Figure 2B). Moreover, RNA yields were comparable between fixed and non-fixed T3-SCs (Figure 2C). In order to extend our comparison, the extracted RNA was subjected to next-generation RNA sequencing (RNA-seq). Analysis of the distribution of the sequencing reads to all genes showed no 5′ or 3′ bias for the fixed or the non-fixed T3-SCs, further indicating that the fixation protocol did not interfere with RNA integrity (Figure 2D). Also, the mRNA composition of fixed and live T3-SCs transcriptomes were highly similar, as only 3 differentially expressed genes were identified (Figure 2E). Finally, the simple error ratio estimate (SERE) statistic (Schulze et al., 2012) and principal-component analysis demonstrated high similarity between live and fixed T3-SCs (Figures 2F, S2A, and S2B). In conclusion, the quality and composition of the total RNA extracted from 0.5% PFA-fixated MuSCs is comparable to those from non-fixed cells and suitable for transcriptomic analysis.

Significant Transcriptional Alterations Are Induced during the MuSC Isolation Protocol

We compared the transcripts of T0-SCs (*in situ* fixed), T3-SCs (standard isolation protocol), and time-five (T5)-SCs (Figures 3A and 3B). T5-SC samples were prepared from minced muscles incubated for an additional 2 hr (total preparation, 5 hr) at 37°C, aiming to capture secondary-response genes (Herschman, 1991) (Figure S3A). Of note, both T3- and T5-SCs were fixed following FACS isolation in order to ensure comparability with T0-SC RNA preparations.

Comparison of the T0-, T3-, and T5-SC transcriptomes demonstrated that the standard MuSC isolation procedure induced significant transcriptional changes. Strikingly, a large number of genes showed strong transcript inductions during

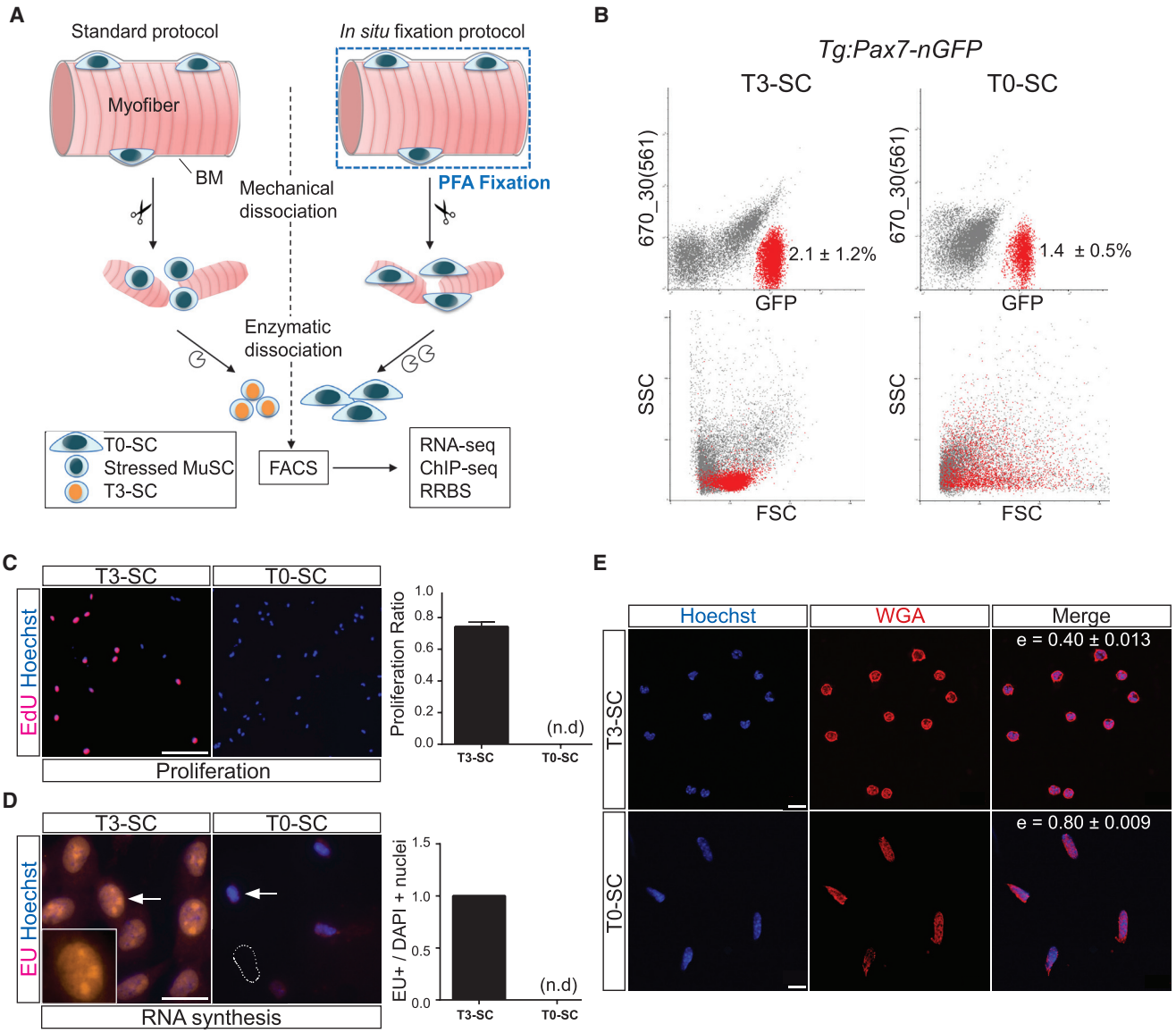

Figure 1. Isolation of MuSCs in a Fixed, G0-Arrested State

(A) Graphical scheme of the *in situ* fixation protocol for MuSCs isolation and comparison to the standard protocol. A detailed description of the protocols is available in the Supplemental Information. BM, basement membrane; T0-SC, time-zero/quiescent MuSC; T3-SC, time 3 hr/activated MuSC.

(B) FACS profiles of non-fixed (T3-SC) and fixed (T0-SC) GFP$^+$ MuSCs from *Tg:Pax7-nGFP* muscle preparations. Sorted GFP$^+$ cells are marked as red dots in all plots. SSC, side scatter, FSC, forward scatter. Values on the plots indicate mean percentage of sorted GFP$^+$ cells of the total number of events, excluding small SSC/FSC and doublets; n = 5.

(C) Proliferation of FACS-isolated T3-SCs and T0-SCs cultured for 48 hr and stained with EdU (24-hr chase); n = 3. EdU$^+$ cells: 0% for T0-SCs and 74% ± 0.03% for T3-SCs.

(D) Nascent RNA synthesis in FACS-isolated T3-SCs and T0-SCs cultured for 48 hr and incubated with labeled ethynyl uridine (EU) ribonucleoside for 2 hr; n = 3. Average of 80 nuclei counted per sample, 100% EU$^+$ and EU$^-$ for T3-SC and T0-SC, respectively. Dotted line delineates cell's nucleus.

(E) Morphology of T3 and T0 MuSCs immediately after the FACS. Cells were spun on Matrigel-coated slides, and membranes were stained with the lectin marker WGA (wheat germ agglutinin). Mean eccentricity of the cells was computationally calculated (Experimental Procedures).

Data are reported as mean ± SD; n.d, not detected. Scale bars, 90 μm in (C), 20 μm in (D), 8 μm in (D, insets), and 10 μm in (E). See also Supplemental Information.

the isolation (2,822 T3/T0 upregulated genes with a fold change [FC] > 2 and a false discovery rate [FDR] < 0.05), whereas the changes were moderate between the T3 and T5 time points (222 T5/T3 upregulated genes; FC > 2, and FDR < 0.05) (Figures 3A, 3B, and S3B; Table S1). Of interest, a large number of transcripts was downregulated during the isolation process (4,840 T3/T0 downregulated genes; FC > 2, and FDR < 0.05), suggesting that RNA degradation mechanisms, in addition to attenuation of transcription, may operate at the early phases of MuSC activation.

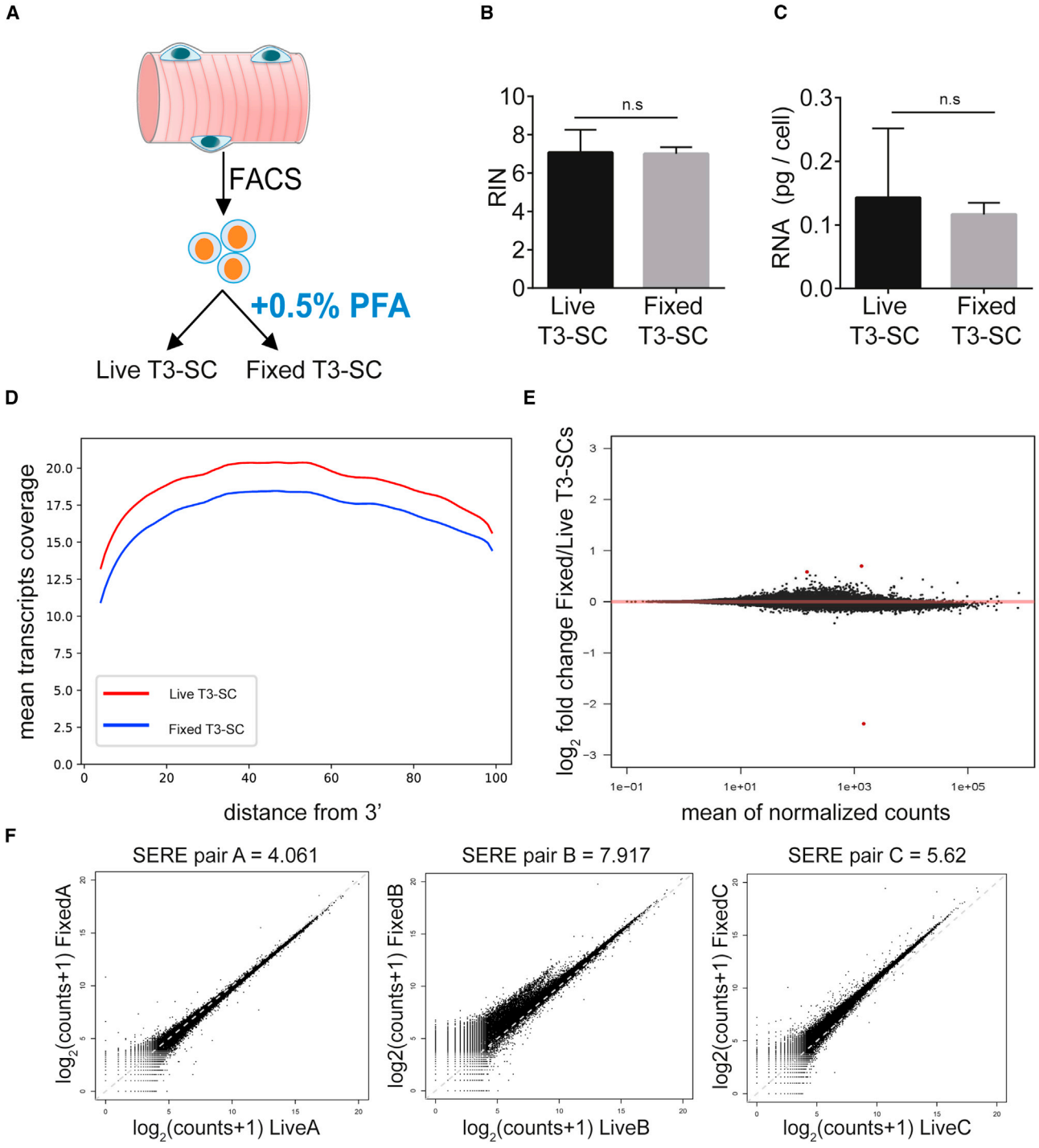

Figure 2. Assessment of the Effects of PFA Fixation on RNA Quality and Composition

(A) Graphical scheme of the procedure for the isolation of non-fixed (Live T3-SC) and fixed MuSCs (Fixed T3-SC). Following the standard protocol, half of the FACS-isolated MuSCs were fixed in 0.5% PFA for 30 min, and total RNA was extracted and compared to that of live T3-SCs.

(B) Mean RNA integrity numbers of live and fixed T3-SCs.

(C) Mean of total RNA recovered per cell in live and fixed T3-SCs preparations, calculated with the Bioanalyzer 2100.

(D) Normalized distribution of the sequencing reads to the predicted transcripts length (5′ to 3′).

(legend continued on next page)

Gene ontology analysis for biological processes of the T3/T0 upregulated genes (early response and dissociation-induced genes) showed a transcriptional signature consistent with a transition from quiescence to activation and proliferation, with enriched rRNA maturation and cell-cycle re-entry terms (Figure 3C; Table S1). Instead, the signature of the T3/T0 downregulated transcripts (quiescence-enriched genes) included genes related to fatty-acid metabolism, in agreement with the metabolic switch from fatty-acid oxidation to glycolysis taking place during MuSC activation (Ryall et al., 2015) (Figures 3C and 3D). The GO analysis also highlighted genes related to cilia as quiescence enriched, a structure described to be present in quiescent MuSCs but disassembled in the activated cells (Jaafar Marican et al., 2016) (Figure 3C).

The comparison between the T0 and T3 transcriptomes identified MuSC activation-induced genes already described, validating our approach but also revealing that these changes occur earlier than previously estimated. Within just 3 hr, the downstream targets of Notch signaling *Hes1* and *HeyL* were decreased by 5- and 8-fold, respectively, consistent with what has been reported for *in-vivo*-activated MuSCs at 20 hr post-injury (Mourikis et al., 2012). Similarly, the hallmark MuSC gene *Pax7*, whose encoded protein marks both stem and progenitor muscle cells, was found 10-fold downregulated in T3-SCs, supporting a quiescence-specific function of this paired-type homeodomain transcription factor. Instead, expression of the muscle regulatory factor *Myod* was rapidly upregulated 10-fold in T3-SCs. As shown in Figure 3D, the dissociation procedure also induced the expression of early response genes, which are known to be transiently activated in response to a variety of stimuli (Herschman, 1991). Among these, we found members of the *Immediate early response Ier-2*, *-3*, *-5*, and *-5l* and *Early growth response* genes *Egr-1*, *-2*, and *-3*. Also, in the T3-SCs, which correspond to the MuSCs isolated to date by the standard protocols, we found an over-representation of a number of oncogenes, like *c-myc* and *Maff* and also members of the AP-1 transcription factor family, like *c-Fos*, *c-Jun*, and others (Figure 3D). To investigate the functional role of AP-1 in the early activation of quiescent MuSCs, we incubated freshly isolated cells in the presence of the pathway inhibitor SR-11302 (Fanjul et al., 1994; Huang et al., 1997). We found that SR-11302 resulted in a 3-fold decrease of proliferating cells after 48 hr in culture, indicating that AP-1 is involved in the exit of MuSCs from quiescence (Figures S3C and S3D).

The *in-situ*-fixed MuSC transcriptome enabled us to identify potentially important quiescence factors that were previously missed, due to their sharp downregulation during the isolation process. Of interest, we uncovered a substantial number of zinc finger protein-encoding genes (223 in total [FC > 2, and FDR < 0.05], of which 143 had at least one transcriptional repression Krüppel Associated Box (KRAB) domain and 182 had at least one DNA-binding zinc finger C2H2 type [ZNF-C2H2] motif). Also, we identified a large group of *Hox-a*, *-b*, and *-c* genes and, further, confirmed them as quiescence specific. We validated by immunofluorescence the differential expression of HOXA9, which we found present in quiescent but absent in activated MuSCs following muscle injury (Figure 3E). Our observation suggests a role of HOXA9 in quiescence, extending a recent study that found HOXA9 absent in freshly isolated and activated MuSCs (Schwörer et al., 2016).

Paradoxically, several proto-oncogenes, including the AP-1 members, have been proposed as quiescence enriched, based on comparisons between freshly isolated and tissue-cultured or *in-vivo*-activated and even proliferating MuSCs (Fukada et al., 2007; Liu et al., 2013; Pallafacchina et al., 2010). In fact, on average, 21% of the microarray-based quiescent signatures reported in the literature (transcripts enriched in freshly isolated MuSCs, FC > 5) correspond to genes that we found as specific for the T3-SC transcripts (Figure 3F) and, hence, are not quiescence-related genes but, instead, consist of early-activation- and isolation-induced artifacts. Of note, the fact that these genes were found at higher levels in the freshly isolated cells than in the activated and/or proliferating cells indicates that they could constitute transiently and highly induced transcripts, a characteristic feature of early-response genes (Amit et al., 2007).

Overall, only 34%, on average, of the T0/T3 downregulated transcripts were present in the microarray-based published quiescent signatures reported earlier (Figure 3F) and 16% in a more recent RNA-seq-based study (Ryall et al., 2015) (Figure 3G). Taken together, despite any bias introduced by technical and biological differences among samples, these comparisons underscore the fact that the majority of the quiescence-enriched transcripts that we identified by the *in situ* fixation technique were missed by the standard protocols. Overall, our data highlight that the presumably quiescent MuSCs isolated and analyzed to date are, in fact, already activated, with a transcriptional profile that diverges significantly from that of the MuSCs in their niche *in vivo*.

The *In Situ* Fixation Protocol Is Compatible with MuSC-Antibody-Based Cell Sorting

To validate the adequacy of our *in situ* fixation protocol for the isolation of cells devoid of transgenic fluorescent markers, we applied antibody-based cell sorting of T0- and T3-SCs, using a published protocol (Pannérec et al., 2013; Figure 4A). Both T0- and T3-SC populations sorted with this strategy presented a similarly high purity of MuSCs, as assessed by PAX7 immunostaining (94% ± 0.6% and 94% ± 1.9 for T0- and T3-SCs, respectively) (Figures 4B and 4C). To ensure that the transcriptomic changes observed by the T0/T3 comparisons from *Tg:Pax7-nGFP* muscles were reproducible on antibody-sorted MuSCs, we performed qRT-PCR analysis on a set of 24 differentially expressed genes (12 up- and 12 downregulated genes). Notably, all tested transcripts displayed a highly similar pattern and level of expression in the antibody-sorted T0- and T3-SCs, compared to their GFP^+-sorted counterparts (Figure 4D). Using

(E) MA plot of live versus fixed T3-SCs RNA-seq data. Only three significantly deregulated transcripts (FDR < 0.05) were identified and are highlighted in red; n = 3.
(F) Simple error ratio estimate (SERE) coefficient for the three sets of paired live and fixed T3-SC RNA-seq samples (pairs A, B, and C). For comparison, a matrix table with the SERE coefficients between all the samples used in this study is shown in Figure S2A.
n.s, not significant. Data are reported as mean ± SD. See also Figure S2.

A

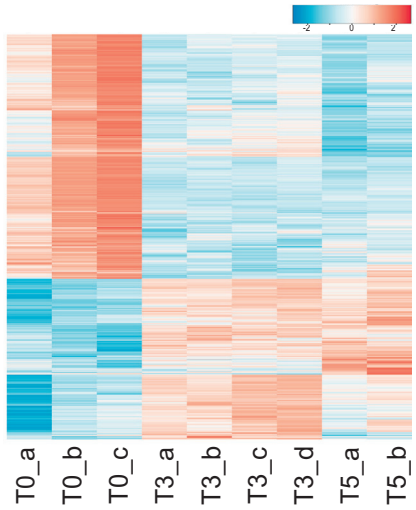

B

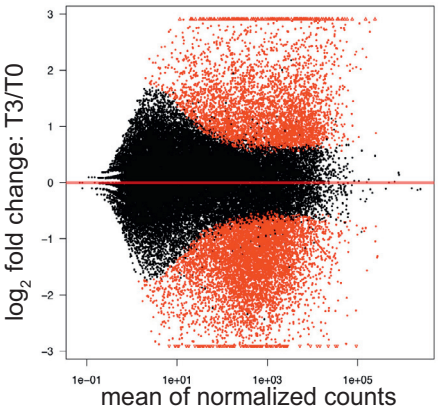

C

Upregulated in T3-SC	Downregulated in T3-SC
maturation of LSU-rRNA	intraciliary transport
regulation of macrophage differentiation	protein transport along microtubule
cellular response to interferon-beta	microtubule-based protein transport
ribosomal large subunit biogenesis	GPI anchor biosynthetic process
regulation of transcription from RNA polymerase II promoter in response to stress	non-motile cilium assembly
maturation of SSU-rRNA	GPI anchor metabolic process
response to interferon-beta	smoothened signaling pathway
regulation of DNA-templated transcription in response to stress	phosphatidylinositol biosynthetic process
translational initiation	mitochondrial respiratory chain complex assembly
ribosomal small subunit biogenesis	protein complex localization
G1/S transition of mitotic cell cycle	fatty acid catabolic process
cell cycle G1/S phase transition	monocarboxylic acid catabolic process

D

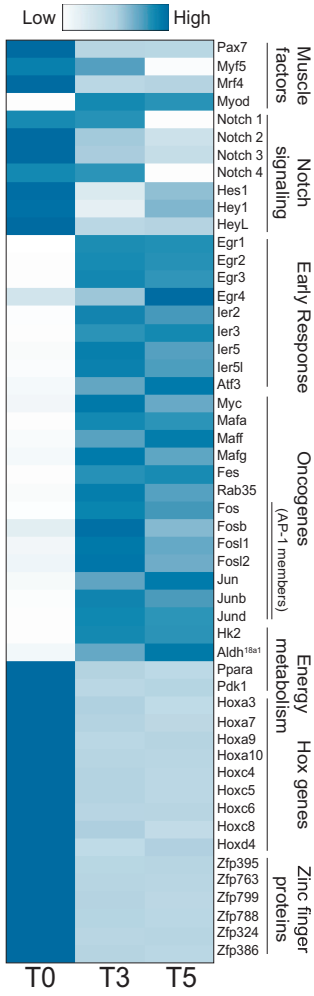

E

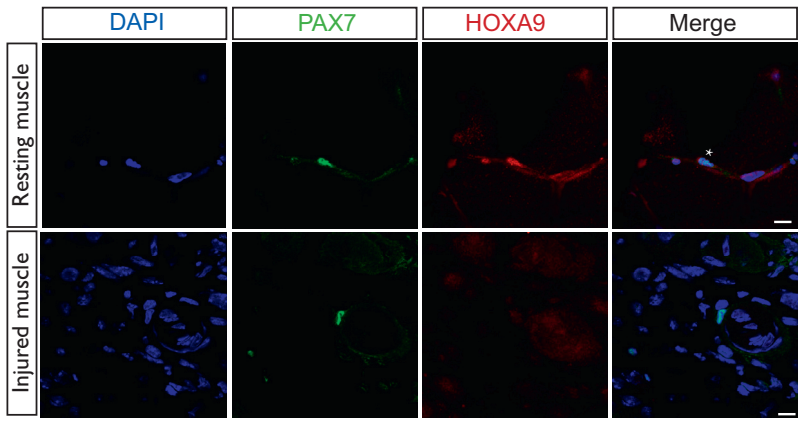

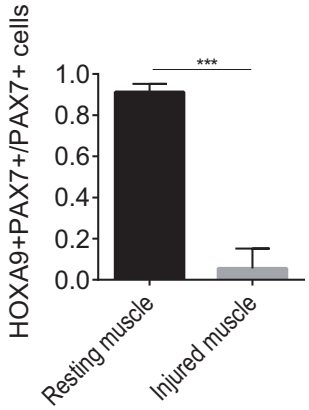

F

T3 up- or down- regulated vs MuSCs quiescence microarrays

	Fukada et al. 2007	Pallafacchina et al. 2010	Liu et al. 2013
T3-SCs up	208 (22%)	239 (26%)	132 (15%)
T3-SCs down	332 (34%)	257 (28%)	351 (40%)
Total	966	906	870

G

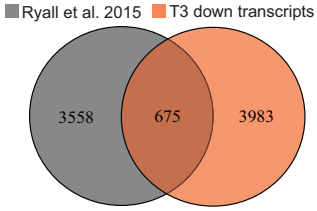

(legend on next page)

two completely independent approaches (RNA-seq on GFP$^+$ cells from *Tg:Pax7-nGFP* mice and qRT-PCR on antibody-sorted cells), we obtained the same gene responses, thus cross-validating the RNA-seq results and the antibody-based isolation on fixed MuSCs. In conclusion, the *in situ* fixation protocol is compatible with antibody-based cell sorting for the aforementioned antigens and, depending on the antigens, should be applicable to other sorting strategies.

MuSC Isolation Protocols Induce Specific Histone Modification Changes but No DNA Methylation Changes

A comprehensive characterization of the epigenetic landscape of a cell allows the functional annotation of the genome and delineates the determinants of cell identity (Barrero et al., 2010). Histone modifications and DNA methylation are among the most studied epigenetic alterations. To gain insights on the epigenetic features of quiescent MuSCs, the quiescence-to-activation transition, but also to investigate the compatibility of the *in situ* fixation protocol to diverse high-throughput techniques, we performed chromatin immunoprecipitation (ChIP) sequencing (ChIP-seq) for histone H3 modifications and DNA methylation analysis by reduced representation bisulfite sequencing (RRBS) on T0-SCs and T3-SCs.

H3 lysine 4 trimethylation (H3K4me3) is a marker of active transcription on promoters (Barski et al., 2007), while acetylation on lysine 27 (H3K27ac) has been associated with active enhancers (Creyghton et al., 2010). Other H3 modifications have been linked to transcriptional repression, such as H3K27me3, which is associated with promoters of silenced genes (Barski et al., 2007). Of interest, we observed that the isolation procedure was sufficient to induce a global increase of H3K4me3 on promoters (Figure 5A; Table S2), concomitantly with a decrease of H3K27ac levels on distal enhancers (Figure 5B; Table S2). In T3-SCs, we identified 14,518 promoters with H3K4me3 peaks, compared to 11,597 promoters in the quiescent T0-SCs. Of note, during the isolation procedure, essentially all (99.9%) H3K4me3-labeled promoters kept their methylation mark, and many (2,936) newly labeled promoters were identified (Figure 5A). Representative examples of gain of H3K4me3 at promoters are shown in Figure 5C for *Fosl* and *Egr3,* two primary response genes identified as isolation induced (Figure 3D). Moreover, using H3K27ac ChIP-seq, we found 5,909 genes in T0-SCs and 4,031 in T3-SCs with at least one associated active distal enhancer (Figure 5B). Similarly, examples of net decrease of H3K27ac are shown in Figure 5D, around the Notch signaling downstream target *Hes1* and the MuSCs hallmark gene *Pax7*.

The observation that almost every H3K4me3$^+$ promoter in T0-SCs is also labeled in T3-SCs indicated that transcriptional silencing induced during isolation is not mediated by the loss of H3K4me3. Gain of repressive marks, such as H3K27me3, could provide an alternative mechanism of transcriptional repression, although its presence in MuSCs is controversial (Boonsanay et al., 2016; Liu et al., 2013). Our ChIP-seq results indicate that MuSCs have almost undetectable levels of H3K27me3, consistent with previous immunofluorescence and ChIP-seq data (Liu et al., 2013), (Figure 5E).

DNA methylation is generally associated with gene silencing (Miranda and Jones, 2007), although the exact effect of methyl groups on enhancers or promoters and transcriptional activity is complex (King et al., 2016). We assessed whether the DNA methylation status in MuSCs was different between T0-SCs and T3-SCs. RRBS, however, detected just 21 out of the 27,878 CpG clusters interrogated as differentially methylated (Figure 5F; Table S2), suggesting that DNA methylation is not a driving force of the transcriptional variations that we observed.

DISCUSSION

The stem cell niche is a critical determinant of a cell's properties. However, all the parameters that constitute the microenvironment are drastically altered when a cell is isolated. Therefore, we hypothesized that the molecular profile of a freshly isolated cell is significantly different from that encountered in its tissue of origin. Indeed, an elegant study, published recently, showed with single-cell analysis on MuSCs that a number of changes do occur during isolation at the levels of transcription and mitochondrial metabolism (van den Brink et al., 2017). In an era when biologists rely increasingly on next-generation sequencing and molecular profiling of cells to study biological phenomena, the isolation-induced alterations could constitute a major technical pitfall for many studies. For transcriptomic analysis, several methods have been developed to overcome this problem. Most of these studies rely on microscopy to infer the composition and topological distribution of transcripts (Chen et al., 2017; Lee et al., 2015; Peng et al., 2016). However, these methods remain technically challenging, costly, and with limited gene coverage. To address this problem, we have developed an

Figure 3. Drastic Transcriptional Changes Occurring during the Dissociation and Early Activation of MuSCs

(A) Heatmap of 12,582 differentially expressed transcripts between T0-SC, T3-SC, and T5-SC based on RNA-seq.

(B) MA plot of T3-SC over T0-SC RNA-seq data. Significantly deregulated transcripts (FDR < 0.05) are highlighted in red; n = 3 for T0, and n = 4 for T3.

(C) Gene ontology for biological processes of the up- and downregulated genes. Top 12 enriched terms are presented. All p values < 0.05; individual p values are given in Table S1.

(D) Heatmap showing average number of normalized reads of T0-SC, T3-SC, and T5-SC RNA-seq data for a selection of genes. n = 3 for T0, n = 4 for T3, and n = 2 for T5.

(E) Immunostaining of PAX7, HOXA9 and DAPI in resting TA muscles or after cardiotoxin injection (4 days post injury). The arrows indicate PAX7$^+$ MuSCs. Scale bars, 10 μm. Quantification is shown on the right. n = 3; ***p < 0.001; data are reported as mean ± SD.

(F) Comparison between the T3 and T0 differentially expressed transcripts (both directions) and three published MuSC quiescent signatures based on microarrays (Fukada et al., 2007; Liu et al., 2013; Pallafacchina et al., 2010). Percentages depict the overlap of the published quiescent signatures with the T3 and T0 up- or downregulated transcripts (by gene symbols). See Experimental Procedures for details.

(G) Overlap between the gene symbols of the T3 and T0 downregulated transcripts (quiescence enriched) and a published RNA-seq-based quiescence signature (Ryall et al., 2015).

See also Table S1.

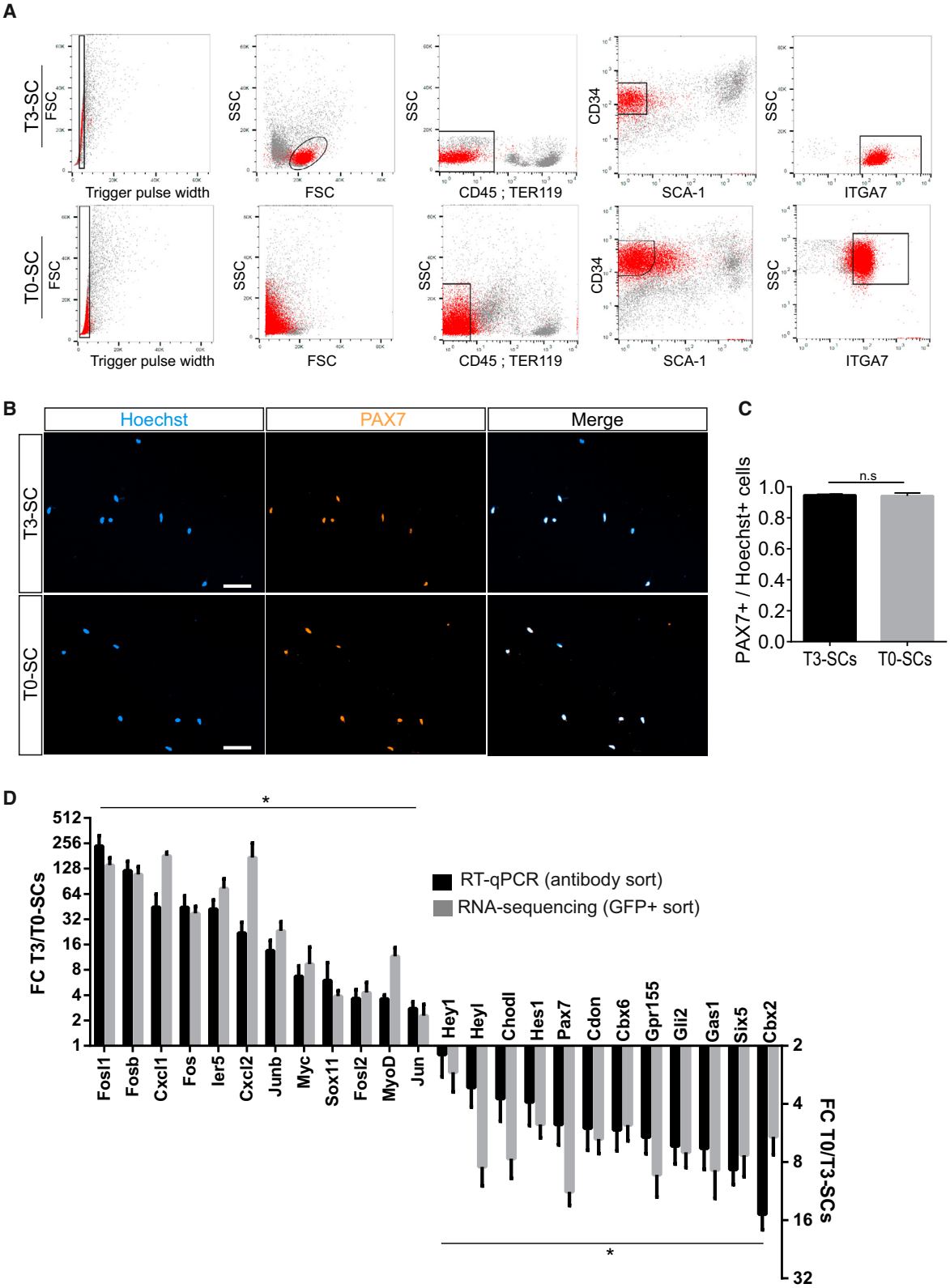

(legend on next page)

in situ fixation, a protocol for the isolation and downstream analysis of quiescent MuSCs. *In situ* fixation preserves the molecular characteristics of isolated MuSCs and is compatible with RNA-seq, ChIP-seq, and RRBS.

The significant transcriptional and epigenetic modifications that we observed demonstrate that the MuSCs isolated by the standard protocols to date have exited quiescence and are already activated. Hence, our results confirmed what the field had suspected for a long time: the extent of alterations that we observed during the dissociation procedure, however, was much greater than previously assumed. Moreover, our findings further underscore the complications of studying quiescence on isolated cells. The development of tissue culture systems that would revert and maintain cells in a true quiescent state would be valuable for dissecting the molecular mechanisms that orchestrate entry, maintenance, and exit from quiescence. Indeed, several groups have made significant progress toward the development of such systems (Arora et al., 2017; Martynoga et al., 2013; Quarta et al., 2016). Quiescence protocols could also be beneficial for cell-based therapies, as the regenerative potential of cultured, activated cells is inferior to freshly isolated MuSCs (Montarras et al., 2005; Sakai et al., 2017).

Applying *in situ* fixation to MuSCs cells permitted us to detect undescribed quiescence and early activation regulators. Using complementary approaches, a study being published concurrently in this issue of *Cell Reports* found similarly that there are transcriptional changes associated with the process of isolation and purification of MuSCs by FACS (van Velthoven et al, 2017). Building reliable quiescent and activation transcriptional and epigenetic signatures, like the ones presented in this report, could provide a valuable source for understanding and manipulating the quiescent state. Quiescent stem cells, like MuSCs, are probably more prone to dissociation-induced signals, as these cells are specialized to get activated for regeneration, in response to disruption of their niche during damage or in pathological conditions. Nevertheless, it is likely that every cell type, especially from cohesive tissues, will be transcriptionally and epigenetically modified during the isolation procedure. As high-throughput characterization is becoming the predominant method of studying and classifying cell types, *in situ* fixation offers an inexpensive and accessible way to improve the accuracy of cellular and molecular analysis.

EXPERIMENTAL PROCEDURES

Isolation of MuSCs from Fixed and Live Tissue

A detailed protocol is described in the Supplemental Information. For the antibody-based cell sorting, the filtered muscle preparations were additionally incubated 45 min on ice with conjugated anti-TER119-PECy7 (1.4 μg/mL; BD Biosciences, #557853), anti-CD45-PECy7 (1.4 μg/mL; BD Biosciences, #552848), anti-CD34-BV421 (5.6 μg/mL; BD Biosciences, #562608), anti-SCA-1-PE (3.5 μg/mL; BD Biosciences, #553108), and anti-ITGA7-Alexa Fluor 700 (0.56 μg/mL; R&D Systems, #FAB3518N) in DMEM (GIBCO)/0.2% BSA. For T0-SCs, the TER119$^-$; CD45$^-$; CD34$^+$; SCA-1$^-$; ITGA7$^+$ cells were sorted. For T3-SCs, the same strategy was used, with the addition of an empirical selection on size and granularity (SSC/FSC).

Mice

Eight- to 12-week-old heterozygous female *Tg:Pax7-nGFP* mice were used to isolate MuSCs (Sambasivan et al., 2009). Animals were handled per French and European Community guidelines.

Muscle Injury

For muscle injury, WT mice were anesthetized with 0.5% Imalgene/2% Rompun, and the tibialis anterior (TA) muscles were injected with 50 μL cardiotoxin (10 mM; Latoxan).

Cell Culture

FACS-isolated T0-SCs and T3-SCs were plated on Matrigel (Corning, #354248)-coated 8-chamber slides (Sarstedt, #94.6140.802) in growth medium (GM) composed of DMEM (GIBCO) with 20% fetal bovine serum (FBS), 1% penicillin/streptomycin (PS; GIBCO), and supplemented with 5 ng/μL basic FGF (bFGF; Peprotech, #450-33) at 37°C. To measure proliferation, after 24 hr in culture, cells were pulsed with 10 μM 5-ethynyl-2′-deoxyuridine (EdU) for 24 hr (EdU Click-iT PLUS Kit C10640, Life Technologies). To assess nascent RNA production, after 46 hr in culture, cells were pulsed with 2 mM 5-ethynyl uridine (EU) for 2 hr (Click-iT nascent RNA imaging kit; Life Technologies, #C10330). EdU and EU labeling was performed according to manufacturer's guidelines. To assess the role of AP-1 pathway activation, the chemical inhibitor SR-11302 (Tocris) was administered at a concentration of 2×10^{-5} M to FACS-isolated MuSCs 24 hr after plating for a duration of 24 hr, including a 4-hr EdU chase.

Immunofluorescence

For cell culture, following fixation (2% PFA, 20 min), MuSCs were washed three times in PBS, permeabilized, and blocked using a blocking solution (BS) containing 2% BSA (Jackson Laboratories), 10% goat serum (GIBCO), and 0.25% Triton X-100 (Sigma) for 30 min at room temperature. The purity of the FACS-isolated cells was assessed with anti-PAX7 antibody (mouse monoclonal; Santa Cruz Biotechnology, #sc-81648) diluted 1:100 in BS and incubated for 16 hr at 37°C. For the membrane staining, WGA was used following manufacturer's guidelines (Thermo Fisher Scientific, #W32464) on T0- or T3-SCs after a 15-min centrifugation (300 × *g*, 4°C) on Matrigel (Corning, #354248)-coated 8-chamber slides (Sarstedt, #94.6140.802).

Cryosections of 10 μm were performed on TA muscles frozen in liquid-nitrogen-cooled isopentane (resting conditions and 4 days post cardiotoxin injury). The sections were fixed in 4% PFA for 15 min at room temperature, permeabilized in cold methanol for 6 min, and boiled in citrate buffer (Dako) for epitope retrieval. To reduce background, the slides were incubated 30 min at room temperature with anti-mouse immunoglobulin G (IgG) Fab fragment (Jackson

Figure 4. Isolation of *In Situ* Fixed MuSCs Using a Combination of Antibodies

(A) FACS profiles of T0 (fixed) and T3 (non-fixed) MuSCs of *Tg:Pax7-nGFP* mice, isolated based on the TER119$^-$; CD45$^-$; CD34$^+$; SCA-1$^-$; Integrin-α7$^+$ selection. Note the scatter pattern of the T0-SCs in the SSC/FSC plot (similar to that in Figure 1B). The GFP$^+$ cells are highlighted in red.

(B) Freshly FACS-isolated T0- and T3-SCs using an antibody cocktail and stained for PAX7. Scale bars, 60 μm.

(C) Quantification of PAX7$^+$ cells in isolated MuSCs: 94% ± 0.6% and 94% ± 1.9% for T0- and T3-SCs, respectively. Data are presented as means ± SD. n.s, not significant.

(D) qRT-PCR analysis on T0 and T3 antibody-based isolated MuSCs for 12 upregulated and 12 downregulated genes (black bars). The targeted transcripts were selected out of the differentially expressed genes from the T0- and T3-SCs RNA-seq analysis (gray bars). For qRT-PCR, data are presented as normalized T3/T0 transcript ratios ($2^{-\Delta\Delta Ct}$) using the mean of *Tbp1* and *Hprt* housekeeping genes. FC, fold change. Data are presented as means ± SD. *$p < 0.05$, with a correction for a FDR of 5%.

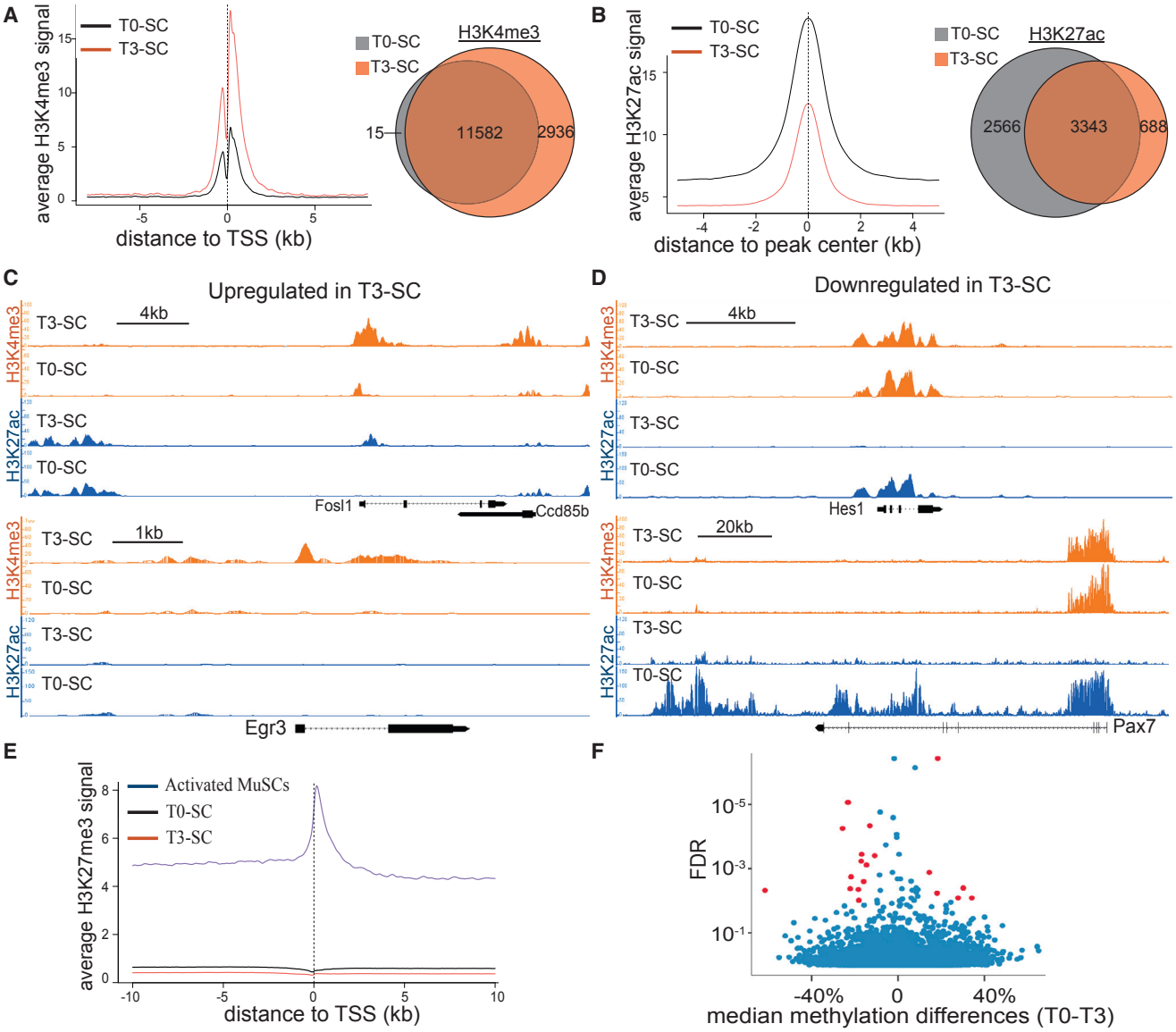

Figure 5. Histone H3 Modifications and DNA Methylation during Early MuSCs Activation

(A) Left: H3K4me3 ChIP-seq averaged signal at promoters. Right: overlap between T0-SC and T3-SC genes with H3K4me3 peaks at promoters. TSS, transcription start site.

(B) Left: H3K27ac ChIP-seq averaged signal at active distal enhancers (H3K27ac peaks outside gene body) from T0-SC and T3-SC samples. Right: overlap of genes that present at least one distal enhancer between T0-SCs and T3-SCs.

(C) Examples of H3K4me3 and H3K27ac ChIP-seq tracks from T3 and T0 upregulated genes *Fosl* and *Egr3*.

(D) Examples of H3K4me3 and H3K27ac ChIP-seq tracks from T3 and T0 downregulated genes *Hes1* and *Pax7*.

(E) H3K27me3 ChIP-seq averaged signal at promoters between T0-SCs, T3-SCs, and activated MuSCs from a published dataset (Liu et al., 2013).

(F) Volcano plot representing genomic DNA methylation changes between T0-SCs and T3-SCs. Each dot represents one of 27,878 CpG clusters interrogated. Among all clusters (blue), those with a methylation change $\geq$ 10% and an FDR < 0.01 were considered significantly different (red). FDR, false discovery rate (logarithmic scale).

Laboratories) at a 1:50 dilution. The blocking was performed for 1 hr at room temperature in 5% BSA. The following primary antibodies were used: anti-HOXA9 (Millipore 07-178) and anti-PAX7 (Santa Cruz, #sc-81648), all at a dilution of 1:100. Incubation with primary antibodies was performed overnight at 4°C. Secondary antibody incubation was performed for 1 hr at room temperature (Thermo Fisher Scientific, Alexa Fluor secondary antibodies diluted at 1:500), and DAPI staining was performed for 10 min at room temperature at 0.5 μg/mL.

Image Analysis

Images were acquired using AxioImager D1, a Zeiss microscope, or a Leica LSM 800 confocal microscope. The eccentricity of the cells, defined as the ratio of the distance between the foci of the ellipse and its major length axis, was calculated using CellProfiler (http://cellprofiler.org/) after automatically drawing all WGA-positive areas per field and filtering out the ones without Hoechst-positive areas inside using an in-house pipeline. A minimum of 100 cells have been analyzed per replicate.

DAPI Incorporation by MuSCs in Total Muscle Preparations

Following enzymatic dissociation and filtering, muscle preparations were incubated on ice for 50 min with 1 μg/mL DAPI. A minimum of 1 × 10^3 cells per replicate was analyzed using the BD Influx Software.

RNA Extraction

A minimum of 2.5 × 10^5 cells per replicate were isolated by FACS. Cells were washed three times with cold PBS, and RNA was extracted using the RecoverAll Kit for FFPE (Ambion, #AM1975) following the manufacturer's guidelines, with slight modifications: the incubation step at 50°C was performed for 1 hr instead of 15 min to improve RNA yield, and the incubation step at 80°C was omitted, as it deteriorated the quality of the recovered RNA, a conclusion also reached by an independent study (Hrvatin et al., 2014). Note that the T3- and T5-SCs were fixed post-FACS isolation for 30 min on ice with 0.5% PFA in PBS to ensure comparability with the fixed T0-SCs. For the experiments in Figure 2, the live T3-SCs were not fixed prior to RNA isolation, and for these samples, the 50°C incubation step was performed for 15 min instead of 1 hr.

qRT-PCR

Reverse transcription was performed using the SuperScript III Reverse Transcriptase kit (Thermo Fisher Scientific, #18080093) with random primers, following the manufacturer's guidelines. qPCR was performed using the Power SYBR Green PCR Master Mix (Applied Biosystems, #4367659). All reactions were run in triplicates and normalized to the mean expression of two housekeeping genes: *Tbp* and *Hprt1*. Primers' sequences are available in Table S3.

High-Throughput Analysis

All procedures related to high-throughput analyses (RNA-seq, ChIP-seq, and RRBS) as well as their corresponding bioinformatics analyses can be found in the Supplemental Experimental Procedures.

Statistical Analysis

For comparison between two groups, unpaired Student's t test was performed to calculate p values and to determine statistically significant differences (*$p < 0.05$; **$p < 0.01$; ***$p < 0.001$). All statistical analyses were performed with GraphPad Prism 6 software. The letter "n" represents biological replicates. A minimum of three independent mice were analyzed for all experiments (except for ChIP-sequencing; see Supplemental Experimental Procedures for details). Data are presented as means ± SD.

DATA AND SOFTWARE AVAILABILITY

The accession numbers for RNA-seq, ChIP-seq, and RRBS raw and processed files are GEO: GSE103162, GSE103163, and GSE104543, respectively, and can be downloaded from the Gene Expression Omnibus website (https://www.ncbi.nlm.nih.gov/geo/) under the accession number GEO: GSE103164.

SUPPLEMENTAL INFORMATION

Supplemental Information includes Supplemental Experimental Procedures, Supplemental *In Situ* Fixation Protocol, three figures, and three tables and can be found with this article online at https://doi.org/10.1016/j.celrep.2017.10.080.

AUTHOR CONTRIBUTIONS

L.M., O.F., J.E.d.L., R.B., F.R., and P.M. designed the experiments. L.M., O.F., J.E.d.L., C.P., A.S., and P.M. performed the experiments. L.M., O.F., J.E.d.L., C.P., R.L., H.V., L.R.I., R.B., F.R., and P.M. analyzed the data. L.M., F.R., and P.M. wrote and edited the manuscript.

ACKNOWLEDGMENTS

We would like to thank A. Guguin and A. Henry of the flow cytometry platform of IMRB, Inserm U955, Creteil. We are grateful to D. Mademtzoglou, M. Gervais-Taurel, A. Prola, D. Hardy, and M. Borok for critical reading of the manuscript and A. Fu for technical assistance. This work was supported by funding to F.R. from the Association Française contre les Myopathies (AFM) via TRANSLAMUSCLE (PROJECT 19507), Labex REVIVE (ANR-10-LABX-73), Fondation pour la Recherche Médicale (FRM; grants FDT20130928236 and DEQ20130326526), Agence Nationale pour la Recherche (ANR) grant Epimuscle (ANR 11 BSV2 017 02), Bone-muscle-repair (ANR-13-BSV1-0011-02), BMP-myomass (ANR-12-BSV1-0038-04), Satnet (ANR-15-CE13-0011-01), Crestnetmetabo (ANR-15-CE13-0012-02), and RHU CARMMA (ANR-15-RHUS-0003). O.F. was a recipient of a research grant from the Danish Diabetes Academy (1077471001) supported by the Novo Nordisk Foundation.

Received: May 11, 2017
Revised: September 13, 2017
Accepted: October 21, 2017
Published: November 14, 2017

REFERENCES

Amit, I., Citri, A., Shay, T., Lu, Y., Katz, M., Zhang, F., Tarcic, G., Siwak, D., Lahad, J., Jacob-Hirsch, J., et al. (2007). A module of negative feedback regulators defines growth factor signaling. Nat. Genet. *39*, 503–512.

Arora, R., Rumman, M., Venugopal, N., Gala, H., and Dhawan, J. (2017). Mimicking muscle stem cell quiescence in culture: methods for synchronization in reversible arrest. In Muscle Stem Cells: Methods and Protocols, E. Perdiguero and D.D.W. Cornelison, eds. (Springer New York), pp. 283–302.

Barrero, M.J., Boué, S., and Izpisúa Belmonte, J.C. (2010). Epigenetic mechanisms that regulate cell identity. Cell Stem Cell *7*, 565–570.

Barski, A., Cuddapah, S., Cui, K., Roh, T.Y., Schones, D.E., Wang, Z., Wei, G., Chepelev, I., and Zhao, K. (2007). High-resolution profiling of histone methylations in the human genome. Cell *129*, 823–837.

Boonsanay, V., Zhang, T., Georgieva, A., Kostin, S., Qi, H., Yuan, X., Zhou, Y., and Braun, T. (2016). Regulation of skeletal muscle stem cell quiescence by Suv4-20h1-dependent facultative heterochromatin formation. Cell Stem Cell *18*, 229–242.

Chen, J., Suo, S., Tam, P.P.L., Han, J.J., Peng, G., and Jing, N. (2017). Spatial transcriptomic analysis of cryosectioned tissue samples with Geo-seq. Nat. Protoc. *12*, 566–580.

Creyghton, M.P., Cheng, A.W., Welstead, G.G., Kooistra, T., Carey, B.W., Steine, E.J., Hanna, J., Lodato, M.A., Frampton, G.M., Sharp, P.A., et al. (2010). Histone H3K27ac separates active from poised enhancers and predicts developmental state. Proc. Natl. Acad. Sci. USA *107*, 21931–21936.

Fanjul, A., Dawson, M.I., Hobbs, P.D., Jong, L., Cameron, J.F., Harlev, E., Graupner, G., Lu, X.P., and Pfahl, M. (1994). A new class of retinoids with selective inhibition of AP-1 inhibits proliferation. Nature *372*, 107–111.

Fukada, S., Uezumi, A., Ikemoto, M., Masuda, S., Segawa, M., Tanimura, N., Yamamoto, H., Miyagoe-Suzuki, Y., and Takeda, S. (2007). Molecular signature of quiescent satellite cells in adult skeletal muscle. Stem Cells *25*, 2448–2459.

Herschman, H.R. (1991). Primary response genes induced by growth factors and tumor promoters. Annu. Rev. Biochem. *60*, 281–319.

Hrvatin, S., Deng, F., O'Donnell, C.W., Gifford, D.K., and Melton, D.A. (2014). MARIS: method for analyzing RNA following intracellular sorting. PLoS ONE *9*, e89459.

Huang, C., Ma, W.Y., Dawson, M.I., Rincon, M., Flavell, R.A., and Dong, Z. (1997). Blocking activator protein-1 activity, but not activating retinoic acid response element, is required for the antitumor promotion effect of retinoic acid. Proc. Natl. Acad. Sci. USA *94*, 5826–5830.

Jaafar Marican, N.H., Cruz-Migoni, S.B., and Borycki, A.-G. (2016). Asymmetric distribution of primary cilia allocates satellite cells for self-renewal. Stem Cell Reports *6*, 798–805.

Jones, N.C., Tyner, K.J., Nibarger, L., Stanley, H.M., Cornelison, D.D.W., Fedorov, Y.V., and Olwin, B.B. (2005). The p38α/β MAPK functions as a molecular switch to activate the quiescent satellite cell. J. Cell Biol. *169*, 105–116.

King, A.D., Huang, K., Rubbi, L., Liu, S., Wang, C.Y., Wang, Y., Pellegrini, M., and Fan, G. (2016). Reversible regulation of promoter and enhancer histone landscape by DNA methylation in mouse embryonic stem cells. Cell Rep. *17*, 289–302.

Lee, J.H., Daugharthy, E.R., Scheiman, J., Kalhor, R., Ferrante, C., Terry, R., Turczyk, B.M., Yang, J.L., Lee, H.S., Aach, J., et al. (2015). Fluorescent in situ sequencing (FISSEQ) of RNA for gene expression profiling in intact cells and tissues. Nat. Protoc. *10*, 442–458.

Liu, L., and Clevers, H. (2010). Coexistence of quiescent and active adult stem cells in mammals. Science *327*, 542–545.

Liu, L., Cheung, T.H., Charville, G.W., and Rando, T.A. (2015). Isolation of skeletal muscle stem cells by fluorescence-activated cell sorting. Nat. Protoc. *10*, 1612–1624.

Liu, L., Cheung, T.H., Charville, G.W., Hurgo, B.M., Leavitt, T., Shih, J., Brunet, A., and Rando, T.A. (2013). Chromatin modifications as determinants of muscle stem cell quiescence and chronological aging. Cell Rep. *4*, 189–204.

Martynoga, B., Mateo, J.L., Zhou, B., Andersen, J., Achimastou, A., Urbán, N., van den Berg, D., Georgopoulou, D., Hadjur, S., Wittbrodt, J., et al. (2013). Epigenomic enhancer annotation reveals a key role for NFIX in neural stem cell quiescence. Genes Dev. *27*, 1769–1786.

Miranda, T.B., and Jones, P.A. (2007). DNA methylation: the nuts and bolts of repression. J. Cell. Physiol. *213*, 384–390.

Mollova, M., Bersell, K., Walsh, S., Savla, J., Das, L.T., Park, S.-Y., Silberstein, L.E., Dos Remedios, C.G., Graham, D., Colan, S., and Kühn, B. (2013). Cardiomyocyte proliferation contributes to heart growth in young humans. Proc. Natl. Acad. Sci. USA *110*, 1446–1451.

Montarras, D., Morgan, J., and Collins, C. (2005). Direct isolation of satellite cells for skeletal muscle regeneration. Science *309*, 2064–2068.

Mourikis, P., Sambasivan, R., Castel, D., Rocheteau, P., Bizzarro, V., and Tajbakhsh, S. (2012). A critical requirement for notch signaling in maintenance of the quiescent skeletal muscle stem cell state. Stem Cells *30*, 243–252.

Pallafacchina, G., François, S., Regnault, B., Czarny, B., Dive, V., Cumano, A., Montarras, D., and Buckingham, M. (2010). An adult tissue-specific stem cell in its niche: a gene profiling analysis of in vivo quiescent and activated muscle satellite cells. Stem Cell Res. *4*, 77–91.

Pannérec, A., Formicola, L., Besson, V., Marazzi, G., and Sassoon, D.A. (2013). Defining skeletal muscle resident progenitors and their cell fate potentials. Development *140*, 2879–2891.

Peng, G., Suo, S., Chen, J., Chen, W., Liu, C., Yu, F., Wang, R., Chen, S., Sun, N., Cui, G., et al. (2016). Spatial transcriptome for the molecular annotation of lineage fates and cell identity in mid-gastrula mouse embryo. Dev. Cell *36*, 681–697.

Quarta, M., Brett, J.O., DiMarco, R., De Morree, A., Boutet, C., Chacon, R., Gibbons, M.C., Garcia, V.A., Su, J., Shrager, J.B., et al. (2016). An artificial niche preserves the quiescence of muscle stem cells and enhances their therapeutic efficacy. Nat. Biotechnol. *34*, 752–759.

Rocheteau, P., Gayraud-Morel, B., Siegl-Cachedenier, I., Blasco, M.A., and Tajbakhsh, S. (2012). A subpopulation of adult skeletal muscle stem cells retains all template DNA strands after cell division. Cell *148*, 112–125.

Rodgers, J.T., King, K.Y., Brett, J.O., Cromie, M.J., Charville, G.W., Maguire, K.K., Brunson, C., Mastey, N., Liu, L., Tsai, C.R., et al. (2014). mTORC1 controls the adaptive transition of quiescent stem cells from G0 to G(Alert). Nature *510*, 393–396.

Rojas-Ríos, P., and González-Reyes, A. (2014). Concise review: The plasticity of stem cell niches: a general property behind tissue homeostasis and repair. Stem Cells *32*, 852–859.

Ryall, J.G., Dell'Orso, S., Derfoul, A., Juan, A., Zare, H., Feng, X., Clermont, D., Koulnis, M., Gutierrez-Cruz, G., Fulco, M., and Sartorelli, V. (2015). The NAD(+)-dependent SIRT1 deacetylase translates a metabolic switch into regulatory epigenetics in skeletal muscle stem cells. Cell Stem Cell *16*, 171–183.

Sakai, H., Fukuda, S., Nakamura, M., Uezumi, A., Noguchi, Y.T., Tajbakhsh, S., and Fukada, S.I. (2017). Notch ligands regulate the muscle stem-like state ex vivo but are not sufficient for retaining regenerative capacity. PLoS One *12*, e0177516.

Sambasivan, R., Gayraud-Morel, B., Dumas, G., Cimper, C., Paisant, S., Kelly, R.G., and Tajbakhsh, S. (2009). Distinct regulatory cascades govern extraocular and pharyngeal arch muscle progenitor cell fates. Dev. Cell *16*, 810–821.

Schulze, S.K., Kanwar, R., Gölzenleuchter, M., Therneau, T.M., and Beutler, A.S. (2012). SERE: Single-parameter quality control and sample comparison for RNA-seq. BMC Genomics *13*, 524.

Schwörer, S., Becker, F., Feller, C., Baig, A.H., Köber, U., Henze, H., Kraus, J.M., Xin, B., Lechel, A., Lipka, D.B., et al. (2016). Epigenetic stress responses induce muscle stem-cell ageing by Hoxa9 developmental signals. Nature *540*, 428–432.

van den Brink, S.C., Sage, F., Vértesy, Á., Spanjaard, B., Peterson-Maduro, J., Baron, C.S., Robin, C., and van Oudenaarden, A. (2017). Single-cell sequencing reveals dissociation-induced gene expression in tissue subpopulations. Nat. Methods *14*, 935–936.

van Velthoven, C.T.J., de Morree, A., Egner, I.M., Brett, J.O., and Rando, T.A. (2017). Transcriptional profiling of quiescent muscle stem cells in vivo. Cell Rep *21*, this issue, 1994–2004.

Zammit, P.S., Golding, J.P., Nagata, Y., Hudon, V., Partridge, T.A., and Beauchamp, J.R. (2004). Muscle satellite cells adopt divergent fates: a mechanism for self-renewal? J. Cell Biol. *166*, 347–357.

Zhang, K., Sha, J., and Harter, M.L. (2010). Activation of Cdc6 by MyoD is associated with the expansion of quiescent myogenic satellite cells. J. Cell Biol. *188*, 39–48.